Journal of Neuroimmunology 330 (2019) 48–54

Contents lists available at ScienceDirect

Journal of Neuroimmunology

journal homepage: www.elsevier.com/locate/jneuroim

A Nurr1 agonist amodiaquine attenuates inflammatory events and neurological deficits in a mouse model of intracerebral hemorrhage

Keita Kinoshita[a], Kosei Matsumoto[b], Yuki Kurauchi[b], Akinori Hisatsune[c,d], Takahiro Seki[b], Hiroshi Katsuki[b,*]

[a] Department of Chemico-Pharmacological Sciences, School of Pharmacy, Kumamoto University, Kumamoto 862-0973, Japan
[b] Department of Chemico-Pharmacological Sciences, Graduate School of Pharmaceutical Sciences, Kumamoto University, Kumamoto 862-0973, Japan
[c] Priority Organization for Innovation and Excellence, Kumamoto University, Kumamoto 860-8555, Japan
[d] Program for Leading Graduate Schools "HIGO (Health life science: Interdisciplinary and Glocal Oriented) Program", Kumamoto University, Kumamoto 862-0973, Japan

ARTICLE INFO

Keywords:
Hemorrhagic stroke
Nuclear receptor
Microglia
Astrocyte
Motor dysfunction

ABSTRACT

Inflammatory responses are considered to play pivotal roles in the pathogenesis of intracerebral hemorrhage (ICH). Here we show that a nuclear receptor Nurr1 (NR4A2) was expressed prominently in microglia/macrophages and astrocytes in the perihematomal region in the striatum of mice after ICH. Daily administration of a Nurr1 agonist amodiaquine (40 mg/kg, i.p.) from 3 h after ICH induction diminished perihematomal activation of microglia/macrophages and astrocytes. Amodiaquine also suppressed ICH-induced mRNA expression of IL-1β, CCL2 and CXCL2, and ameliorated motor dysfunction of mice. These results suggest that Nurr1 serves a novel target for ICH therapy.

1. Introduction

Intracerebral hemorrhage (ICH), a neurological disorder initiated by rupture of blood vessels and leakage of blood constituents into brain parenchyma, is associated with poor prognosis such as high mortality and severe deficits in sensorimotor functions (Cordonnier et al., 2018). Development of effective drug therapies to avoid these severe conditions has been anticipated but not yet achieved. Accumulating lines of evidence indicate that inflammatory events play pivotal roles in the pathogenic processes of ICH and therefore are considered to serve potential therapeutic targets (Zhou et al., 2014). Inflammatory events in ICH are characterized by activation and accumulation of brain-resident microglia and astrocytes, in addition to infiltration of monocytes/macrophages and other myeloid cells, around and into the hematoma. Indeed, we have previously reported that several drugs inhibited mobilization and/or activation of these inflammatory cells and ameliorated neurological outcome after ICH (Matsushita et al., 2011; Hijioka et al., 2017).

Nurr1 (NR4A2) is a member of nuclear receptor family that is predominantly expressed in the central nervous system (Law et al., 1992). Initially, the physiological role of Nurr1 as a regulator of midbrain development has been highlighted because gene deletion of this nuclear receptor results in failure of generation of midbrain dopaminergic neurons (Zetterström et al., 1997; Perlmann and Wallén-Mackenzie, 2004). In addition, dopaminergic neurons in adult heterozygous Nurr1 knockout mice are more susceptible to neurotoxic insults than those in wild-type mice, indicating that Nurr1 may also regulate neuronal viability (Le et al., 1999). Notably, this nuclear receptor may also act as a regulator of inflammatory responses in the brain. For example, Nurr1 gene expression is induced in response to lipopolysaccharide (LPS) in microglia (Fan et al., 2009). A study by Saijo et al. (2009) has demonstrated that Nurr1 plays an anti-inflammatory role by suppressing the release of inflammatory mediators from microglia and astrocytes.

Although Nurr1 has been recognized as a constitutively active nuclear receptor due to the unique structure of its ligand-binding domain (Wang et al., 2003), several compounds have been found to act as Nurr1 ligands (Inamoto et al., 2008) and attenuates the cytotoxicity of dopaminergic neurotoxin (De Miranda et al., 2015b). In this context, amodiaquine is a 4-aminoquinoline class of antimalarial drug that has recently been demonstrated to possess agonistic activity on Nurr1 and thereby protect dopaminergic neurons in a mouse model of Parkinson's disease (Kim et al., 2015). Whether Nurr1 activation by chemical compounds such as amodiaquine is effective in ameliorating neurological disorders other than Parkinson's disease has not been examined. In the present study, we addressed whether Nurr1 can serve a therapeutic target for ICH, by examining the effect of amodiaquine on an

* Corresponding author at: Department of Chemico-Pharmacological Sciences, Graduate School of Pharmaceutical Sciences, Kumamoto University, 5-1 Oe-honmachi, Kumamoto 862-0973, Japan.
E-mail address: hkatsuki@gpo.kumamoto-u.ac.jp (H. Katsuki).

https://doi.org/10.1016/j.jneuroim.2019.02.010
Received 23 December 2018; Received in revised form 5 February 2019; Accepted 21 February 2019

experimental model of ICH in mice.

2. Materials and methods

2.1. Animals

Male ICR mice (Nihon SLC, Shizuoka, Japan) at 8 to 10 weeks of age were used in all experiments. All procedures were approved by Kumamoto University ethic committee on animal experiments, and animals were treated in accordance with the Guidelines of the United States National Institutes of Health regarding the care and use of animals for experimental procedures. Animals were maintained at constant ambient temperature (22 ± 1 °C) under a 12-h light/dark cycle (light on between 8:00 AM and 8:00 PM) with food and water available ad libitum.

2.2. ICH induction and drug administration

After intraperitoneal injection of the combination anesthetic consisting of 0.3 mg/kg medetomidine (Zenyaku Kogyo Company, Tokyo, Japan), 4.0 mg/kg midazolam (Astellas Pharma Inc., Tokyo, Japan) and 5.0 mg/kg butorphanol (Meiji Seika Pharma Co., Tokyo, Japan), mice were placed in a stereotaxic frame. A 30-gauge needle was inserted into the striatum through a burr hole on the skull (stereotaxic coordinates: 2.3 mm lateral to the midline, 0.2 mm anterior to the bregma and 3.5 mm depth below the skull). ICH was induced by injection of 0.035 U collagenase type VII (Sigma, St Louis, MO, USA) in 0.5 μl physiological saline, at a constant rate of 0.2 μl/min with a microinfusion pump. Body temperature was maintained at 37 °C during surgery. After surgical operation, mice were returned to their cage and maintained under the same conditions as pre-operation. No death of animals was induced by ICH surgery in the present study. Amodiaquine (cat # CYP526, Cypex Ltd., Dundee, UK) was dissolved in 0.9% physiological saline at 4 mg/ml and administered to mice at 40 mg/kg intraperitoneally, three times in total. Administration was performed at 3 h after induction of ICH and then daily at a 24-h interval. Control animals received vehicle administration.

2.3. Immunohistochemical examinations

At 3 d after ICH induction, mice were anesthetized again with intraperitoneal injection of the combination anesthetic and perfused transcardially with 30 ml of ice-cold phosphate-buffered saline (PBS) followed by 30 ml of 4% paraformaldehyde. Brains were isolated and post-fixed in 4% paraformaldehyde overnight, and then, frozen coronal sections of 16 μm thickness were prepared. Antigen retrieval was performed by incubation in 10 mM citrate buffer (pH 8.0–8.5) for 30 min at 85 °C.

After rinse with PBS containing 0.3% Triton X-100 (PBS/T), specimens were treated with PBS/T and blocking serum for 1 h at 22–25 °C and then incubated with primary antibodies overnight at 4 °C. For detection of Nurr1 expression in neurons, microglia/macrophages and astrocytes, anti-Nurr1 (F-5) (1:1000; cat # SD-376984, Santa Cruz Biotechnology. Inc., Dallas, TX, USA), anti-NeuN (rabbit polyclonal) (1:500; cat# ABN78, Millipore Corporation, Billerica, MA, USA), rabbit anti-Iba1 antibody (1:500; cat# 019–19,741, Wako Pure Chemical, Osaka, Japan), and rabbit monoclonal anti-glial fibrillary acidic protein (GFAP) antibody (1:500; cat# 12389, Cell Signaling Technology) were used as primary antibodies. After rinse with PBS/T, specimens were incubated with the corresponding secondary antibodies for 2 h at 22–25 °C. Secondary antibodies were Alexa Fluor 488 donkey anti-mouse IgG (H + L) antibody (1:1000; Invitrogen™, Life Technologies Japan, Tokyo, Japan) and Alexa Fluor 555 donkey anti-rabbit IgG (H + L) antibody (1:1000; Invitrogen™, Life Technologies Japan). Fluorescence signals were observed with the use of an epifluorescence microscope.

For bright-field examinations of pathological changes in neurons, microglia/macrophages and astrocytes, mouse anti-NeuN monoclonal antibody (1:500; cat # MAB377, Millipore Corporation, Billerica, MA, USA), rabbit anti-Iba1 antibody and rabbit monoclonal anti-GFAP antibody were used as primary antibodies, respectively. In these sets of experiments, secondary antibodies were biotinylated goat anti-mouse IgG (H + L) (1:200; cat # BA-9200, Vector Laboratories, Burlingame, CA) and biotinylated goat anti-rabbit IgG (1:200 or 1:500; cat# BA-1000, Vector Laboratories). After incubation with biotinylated conjugates, specimens were treated with avidin- biotinylated horseradish peroxidase complex (Vectastain Elite ABC kit; Vector Laboratories), and then peroxidase was visualized by diaminobenzidine and H_2O_2. The number of NeuN-immunopositive cells per 270 × 360 μm^2 in individual sections was counted by investigators blinded to the treatment. Five coronal sections collected every 80 μm from each brain were examined for cell counting, and the average number of cells from these sections was taken as the value for each mouse. Quantitation of Iba1-positive cells in the perihematomal region was performed in a similar manner. For GFAP immunoreactivity, threshold-based quantification of the immunopositive area was conducted (Anan et al., 2017) with ImageJ software (National Institutes of Health, Bethesda, MD, USA). The percentage of GFAP-immunopositive area of 270 × 360 μm^2 in the perihematomal region was obtained from each section, and the average percentage from five sections was taken as the value for each mouse.

2.4. Real-time quantitative polymerase chain reaction (RT-qPCR)

At 6 h after ICH, mice were deeply anesthetized and perfused transcardially with 30 ml ice-cold PBS. A brain slice with 4 mm thickness of the hemisphere ipsilateral to the hemorrhage was obtained 2 mm posterior from the frontal pole. The slice was stored in RNAiso Plus reagent (Takara Bio Inc., Shiga, Japan). Total RNA was reverse transcribed into cDNA (1 cycle at 37 °C for 15 min, 85 °C for 5 s) using PrimeScript™ RT Master Mix (Takara Bio Inc.) and used for quantification of mRNAs encoding interleukin (IL)-1β, chemokine C—C motif ligand 2 (CCL2), chemokine C-X-C motif ligand 2 (CXCL2) and IL-15. Glyceraldehyde-3-phosphate dehydrogenase (GAPDH) mRNA was used as internal control. The primers used for RT-qPCR are shown in Table 1. The PCR program was run at 95 °C for 30 s, then 40 cycle at 95 °C for 15 s, 55 °C for 45 s and 72 °C for 30 s. Results were automatically analyzed with a comparative Ct method.

2.5. Estimation of lesion size

The lesion volume was estimated by Nissl staining with Cresyl violet of coronal brain sections of 20 μm thickness obtained every 200 μm. Injured area in sections spanning the entire hematoma was measured by ImageJ software. Hematoma volume was determined by integration of the injured area in each section over the section depth.

Table 1
Primer sequences for quantitative RT-PCR.

Forward	
IL-1β: 5′-TGAAGGGCTGCTTCCAAACC-3′	
CCL2: 5′-GAGGAAGGCCAGCCCAGCAC-3′	
CXCL2: 5′-CGCTGTCATGCCTGAAGAC-3′	
IL-15: 5′-TGCGCCCAAAAGACTTGCAGTG- 3′	
GAPDH: 5′-ACCATCTTCCAGGAGCGAGA-3′	
Reverse	
IL-1β: 5′-TGTCCATTGAGGTGGAGAG-3′	
CCL2: 5′-TGGGCGTTAACTGCATCTGGC-3′	
CXCL2: 5′-CCTTGAGAGTGGCTATGACTTCTG-3′	
IL-15: 5′-TCGTCCAACTCTGCAACTGGGC-3′	
GAPDH: 5′-CAGTCTTCTGGGTGGCAGTG-3′	

2.6. Assessment of motor functions

Motor functions of mice were evaluated by the beam-walking test and the modified limb-placing test, by investigators blinded to the treatments. In the beam-walking test, mice were trained three times before surgery for ICH induction. A beam with 15-mm width, 1.1-m length, and 50-cm height was used. Hindlimb fault rate and walking distance were obtained as the average values from three trials. The performance score of mice was based on an eight-point scale as previously described (Matsushita et al., 2011). Modified limb-placing test consists of two limb placing tasks which assess the sensorimotor integration of the forelimb and the hindlimb, by testing responses to tactile and proprioceptive stimuli as previously described (Matsushita et al., 2011).

2.7. Statistical analysis

All data are presented as means ± S.E.M. Data in Figs. 2 and 4 were analyzed by Student's *t*-test. Data in Figs. 3 and 5 were analyzed by one-way analysis of variance followed by Tukey's multiple comparisons test. Time course data on motor functions in Fig. 6 were analyzed by two-way analysis of variance followed by Bonferroni test. Statistical analysis was carried out with the GraphPad Prism 6 software (Graph Pad, San Diego, CA, USA). Two-tailed probability values < 5% were considered significant.

3. Results

3.1. Nurr1 expression is upregulated in microglia/macrophages and astrocytes in the striatum after ICH

We performed immunofluorescence histochemistry to examine cell types expressing Nurr1 in the brain, using coronal sections corresponding to the location of hematoma. In the intact (contralateral) brain hemisphere, neuronal expression of Nurr1 as revealed by NeuN/Nurr1 double immunofluorescence was observed in a small population of cells distributed in the deep layer of the temporal cortex (Fig. 1A and B). In the same region, Nurr1 immunofluorescence did not merge with Iba1 and GFAP, suggesting specific neuronal expression of Nurr1 in the cortex (data not shown). On the other hand, we observed diffuse distribution of Nurr1 immunofluorescence in the striatum. Double immunofluorescence with Iba1 (Fig. 1C) or GFAP (Fig. 1D) revealed that Nurr1 was expressed in a subpopulation of microglia and astrocytes in the striatum of the contralateral hemisphere. As demonstrated previously (Matsushita et al., 2011; Anan et al., 2017), induction of ICH resulted in robust accumulation of activated microglia/macrophages and astrocytes in the perihematomal region. Within the perihematomal region, activated microglia/macrophages were concentrated in the region nearer to the center of the hematoma, and activated astrocytes were concentrated in the region just outside of the region where activated microglia/macrophages accumulated. We found that, at 3 d after ICH induction, the majority of activated microglia/macrophages and astrocytes in the perihematomal region of the ipsilateral hemisphere exhibited Nurr1 immunofluorescence (Fig. 1C and D).

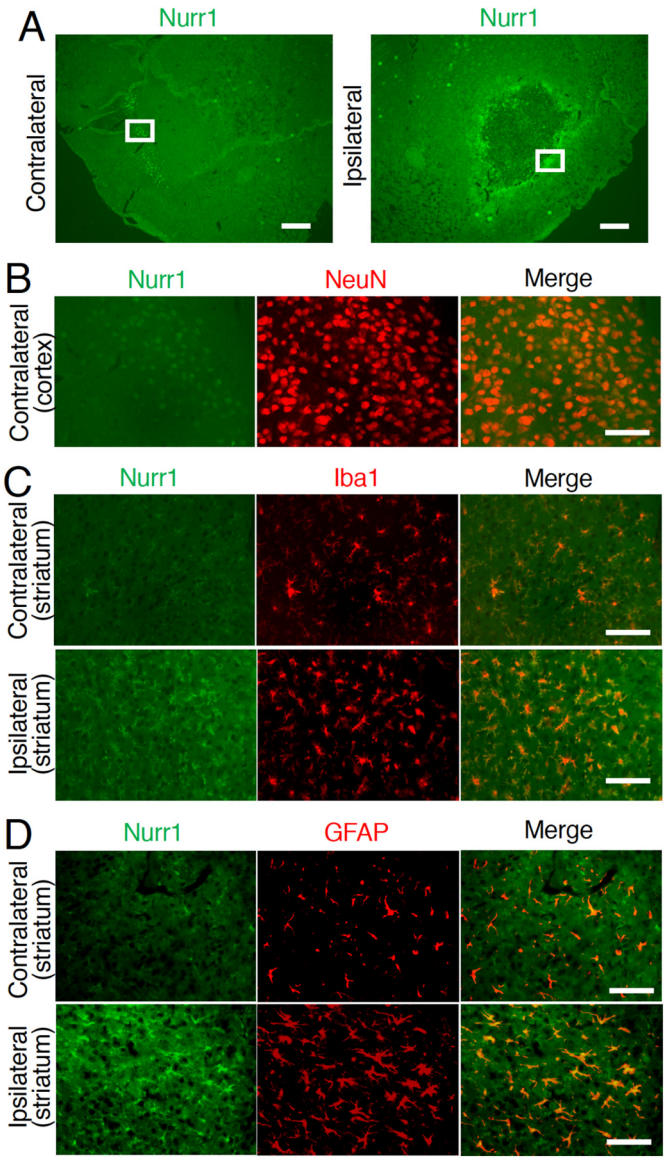

Fig. 1. Nurr1 is expressed in activated microglia/macrophages and astrocytes after ICH induction. Immunofluorescence histochemistry for Nurr1, NeuN, Iba1 and GFAP was performed on coronal brain sections obtained at 3 d after ICH induction. (A) Representative images of Nurr1 immunofluorescence staining in the contralateral hemisphere (left panel) and the ipsilateral hemisphere (right panel). The rectangles indicate the regions corresponding to the magnified views in panels B (the cortex of the contralateral hemisphere) and C – D (the striatum of the ipsilateral hemisphere). Scale bar = 500 μm. (B) Magnified view of double immunofluorescence for Nurr1 (green) and NeuN (red) in the cortex of the contralateral hemisphere. Scale bar = 100 μm. (C) Magnified views of Nurr1 (green) and Iba1 (red) immunofluorescence in the striatum of the contralateral hemisphere and in the perihematomal region of the striatum of the ipsilateral hemisphere. Scale bar = 100 μm. (D) Magnified views of Nurr1 (green) and GFAP (red) immunofluorescence in the striatum of the contralateral hemisphere and in the perihematomal region of the striatum of the ipsilateral hemisphere. Scale bar = 100 μm. (For interpretation of the references to colour in this figure legend, the reader is referred to the web version of this article.)

3.2. Amodiaquine attenuates morphological activation of microglia/macrophages and astrocytes after ICH

Because induced expression of Nurr1 was found prominently in activated microglia/macrophages and astrocytes after ICH, we addressed whether a Nurr1 ligand affected ICH-induced activation of these cells. Mice were treated daily with 40 mg/kg amodiaquine or vehicle, starting from 3 h after induction of ICH. Immunohistochemical detection of Iba1 at 3 d after ICH demonstrated that amodiaquine significantly suppressed accumulation of activated microglia/macrophages in the perihematomal region (Fig. 2A–C). At the same time, activation of astrocytes in the perihematomal region was also suppressed significantly by amodiaquine, as revealed by the drug-induced decrease in GFAP-immunopositive area (Fig. 2D–F).

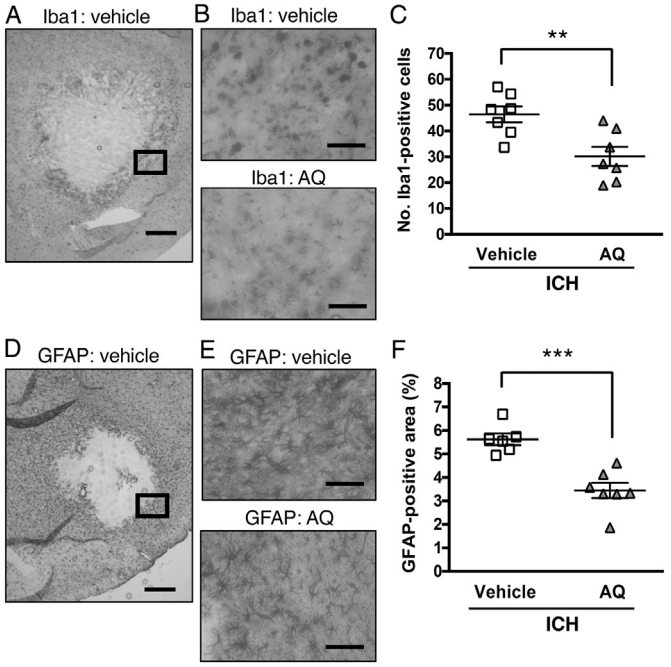

Fig. 2. Amodiaquine attenuates activation of microglia/macrophages and astrocytes by ICH. Amodiaquine (AQ; 40 mg/kg, i.p.) or vehicle was administered 3 h, 27 h and 51 h after induction of ICH. Immunohistochemical examinations on Iba1-positive cells and GFAP-positive cells were performed on coronal brain sections obtained at 3 d after ICH induction. (A) A representative image of Iba1 immunohistochemistry of the ipsilateral hemisphere in a brain section obtained from a vehicle-treated mouse. The rectangle indicates the area used for quantification of Iba1-positive cells. Scale bar = 500 μm. (B) Magnified views of the perihematomal region of brain sections obtained from vehicle- or amodiaquine-treated mice. Scale bar = 100 μm. (C) Results of quantification of Iba1-positive cells in the perihematomal region. Number of animals examined was 6 in ICH ± vehicle group and 7 in ICH ± AQ group, respectively. (D) A representative image of GFAP immunohistochemistry of the ipsilateral hemisphere in a brain section obtained from a vehicle-treated mouse. The rectangle indicates the area used for quantification of GFAP immunoreactivity. Scale bar = 500 μm. (E) Magnified views of the perihematomal region of brain sections obtained from vehicle- or amodiaquine- treated mice. Scale bar = 100 μm. (F) Results of quantification of GFAP-positive area in the perihematomal region. Number of animals examined was 6 in ICH ± vehicle group and 7 in ICH ± AQ group, respectively. ** $P < 0.01$, *** $P < 0.001$.

3.3. Amodiaquine suppresses ICH-induced mRNA expression of inflammatory mediators

Because amodiaquine was found to suppress activation of microglia/macrophages and astrocytes on a morphological basis, we next addressed whether proinflammatory functions of these cells were also suppressed by amodiaquine. For this purpose, we examined mRNA expression levels of several cytokines and chemokines. We confirmed upregulation of mRNAs encoding a proinflammatory cytokine IL-1β and chemokines CCL2 and CXCL2, at 6 h after induction of ICH (Fig. 3A–C). IL-15 has been reported recently as an astrocyte-derived pro-inflammatory cytokine (Li et al., 2016), and we found that IL-15 mRNA was also upregulated in response to ICH (Fig. 3D). Amodiaquine (40 mg/kg), administered at 3 h after ICH induction, significantly suppressed the increase in mRNA expression of IL-1β, CXCL2 and CCL2 (Fig. 3A–C). IL-15 mRNA expression also tended to be suppressed by amodiaquine, but the effect did not reach statistical significance (Fig. 3D).

3.4. Effect of amodiaquine on the injury volume after ICH

Microglia are well known to play an important role in clearance of dead cell debris in damaged brain tissues via their phagocytic activities (Michell-Robinson et al., 2015). Because the hematoma region is occupied by many dead cells of brain parenchyma and blood-derived constituents such as erythrocytes, microglia and infiltrating macrophages are expected to remove them and contribute to the regression of injured brain tissues. To address whether amodiaquine affected the rate of regression of the injured brain tissues, we performed Nissl staining of coronal brain sections to identify the area of tissue injury after ICH (Fig. 4A). Integration of the injured areas of brain sections spanning the entire rostro-caudal levels of hematoma gave the injury volume. As shown in Fig. 4B, the injury volume in vehicle-treated group gradually decreased with time, from 1 d to 7 d after induction of ICH. Amodiaquine treatment produced no significant effect on the injury volume at 1 d and 3 d after ICH. The injury volume at 7 d after ICH tended to be smaller in amodiaquine group than in vehicle group, but the difference did not reach statistical significance.

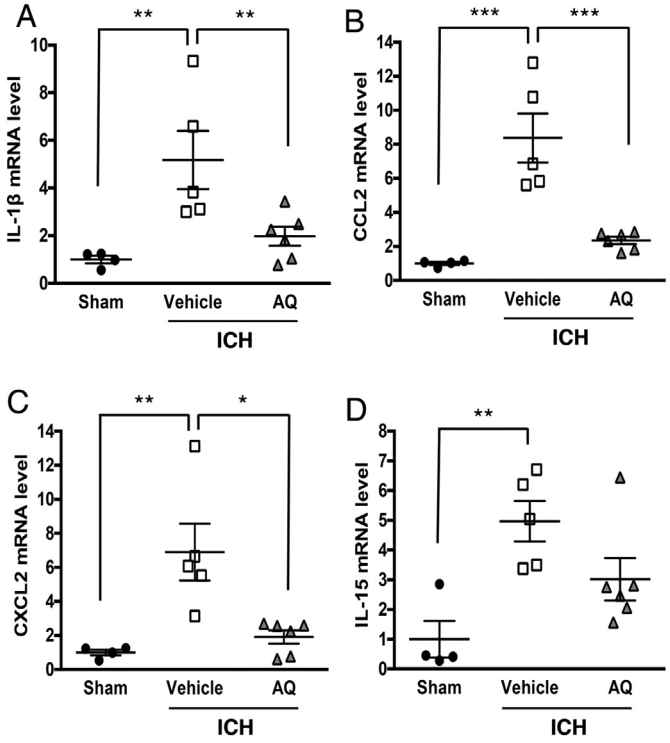

Fig. 3. Amodiaquine suppresses the expression of inflammatory cytokine/chemokine mRNAs associated with ICH.
Amodiaquine (AQ; 40 mg/kg, i.p.) or vehicle was administered 3 h after induction of ICH. RT-PCR analysis of mRNA expression levels of IL-1β (A), CCL2 (B), CXCL2 (C) and IL-15 (D) was performed at 6 h after ICH induction. Sham animals received intrastriatal injection of saline instead of collagenase. Number of animals examined was 4 in vehicle group, 5 in ICH ± vehicle group, and 6 in ICH ± AQ group, respectively. * $P < 0.05$, ** $P < 0.01$, *** $P < 0.001$.

3.5. Effect of amodiaquine on neuronal survival in the hematoma

Nurr1 has been shown to protect midbrain dopaminergic neurons from neurotoxic insults (Le et al., 1999). To determine if Nurr1 activation produced a neuroprotective effect in our experimental ICH model, the number of NeuN-immunopositive cells remaining in the central region of hematoma was quantified at 3 d after ICH. ICH caused a prominent decrease in the number of viable neurons. Daily treatment with amodiaquine (40 mg/kg) did not affect ICH-induced decrease in the number of neurons in the hematoma significantly (Fig. 5).

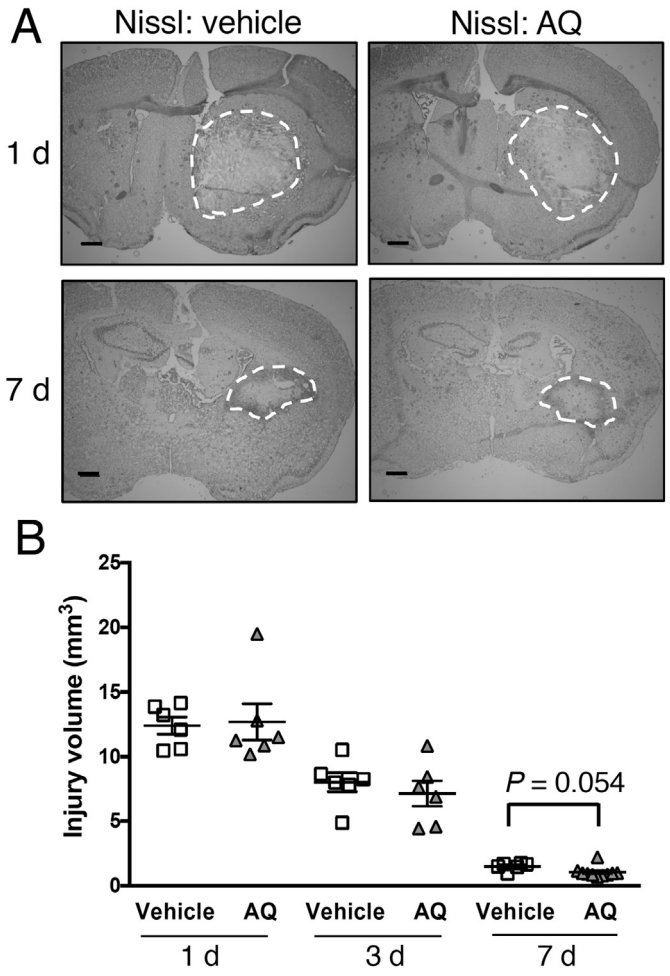

Fig. 4. Amodiaquine modestly affects the injury volume associated with ICH. Amodiaquine (AQ; 40 mg/kg, i.p.) or vehicle was administered 3 h, 27 h and 51 h after induction of ICH. Injury volume was determined by integration of the area damaged by hemorrhage in coronal sections spanning the entire hematoma obtained from individual mice. (A) Representative images of Nissl-stained coronal sections obtained at 1 d and 7 d after ICH induction in vehicle-treated mice and AQ-treated mice. Sections containing the largest area of hematoma at the corresponding time points are shown. Dashed lines encircle the areas damaged by hemorrhage. Scale bars = 500 µm. (B) Quantitative results of the injury volume at indicated periods after induction of ICH. Number of animals examined under each condition was 6, except for the AQ group at 7 d (n = 10).

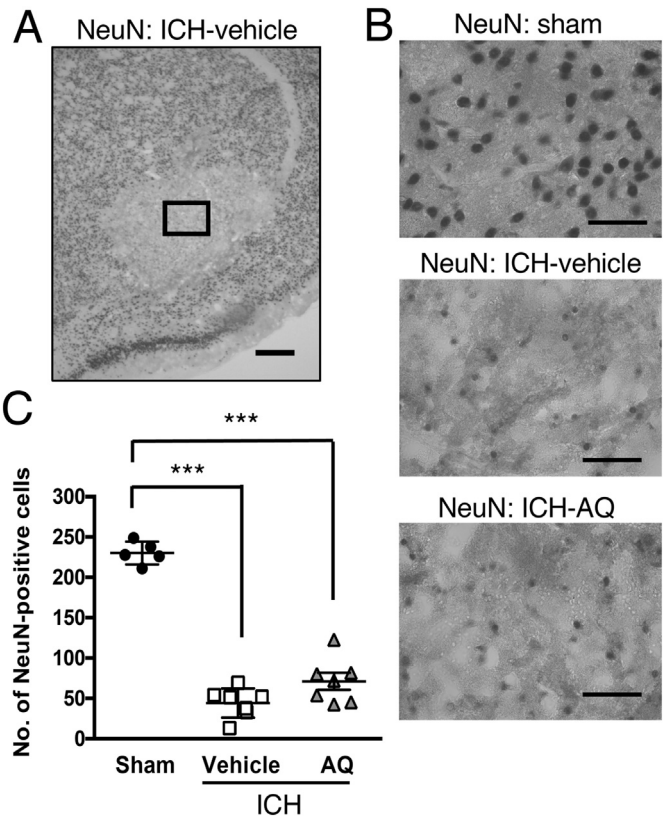

Fig. 5. Amodiaquine minimally affects neuron loss induced by ICH. Amodiaquine (AQ; 40 mg/kg, i.p.) or vehicle was administered 3 h, 27 h and 51 h after induction of ICH. Immunohistochemical examinations on NeuN-positive cells were performed on coronal brain sections obtained at 3 d after ICH induction. (A) A representative image of NeuN immunohistochemistry. The rectangle indicates the area used for quantification of NeuN-positive cells. Scale bar = 500 µm. (B) Magnified views of the regions for quantification in sections obtained from sham-operated mice and mice after ICH with vehicle or amodiaquine treatments. Scale bar = 50 µm. (C) Quantitative results of NeuN-positive cells. Number of animals examined was 5 in vehicle group, 7 in ICH ± vehicle group, and 7 in ICH ± AQ group, respectively. *** P < 0.001.

3.6. Amodiaquine alleviates neurological deficits associated with ICH

Results so far indicated that amodiaquine could ameliorate several pathological parameters after ICH, particularly those related to inflammatory responses. To address whether these effects of amodiaquine were associated with improvement in neurological functions, we examined motor deficits of mice by two kinds of function tests. In the beam-walking test (Fig. 6A), motor dysfunction of mice with vehicle treatment was evident as a drastic increase in the fault rate of hindlimb steps promptly after induction of ICH. The increase in the fault rate continued for 3 d (75 h), and thereafter, the footstep functions exhibited spontaneous recovery to reach comparable level to that of sham-operated mice at 7 d (171 h) after ICH induction. Daily administration of amodiaquine (40 mg/kg) for three times starting from 3 h after induction of ICH resulted in accelerated recovery of footstep functions, and the difference between vehicle group and amodiaquine group was significant at 3 d after ICH induction (Fig. 6A). In the modified limb-placing test (Fig. 6B), the functional deficit was observed for a longer period than in the beam-walking test. The deficit score of vehicle-treated ICH mice remained significantly elevated as compared to sham-operated mice at 7 d after ICH induction. Amodiaquine was effective in lowering the deficit score at 6 h, 3 d and 7 d after ICH.

4. Discussion

The present study was aimed to clarify if Nurr1 could serve a therapeutic target for ICH. Our results demonstrated that Nurr1 expression was upregulated in activated glial cells in the perihematomal region. Importantly, administration of a Nurr1 agonist amodiaquine not only attenuated inflammatory responses associated with glial cell activation, but also improved neurological outcome after ICH.

Expression pattern of Nurr1 in normal brain at developmental and adult stages has already been addressed in several precedent studies. In addition to the midbrain dopaminergic neurons (Bäckman et al., 1999), Nurr1 mRNA has been reported to be expressed in various regions of rat and mouse brains, particularly in deep layers of perirhinal cortex (Honkaniemi et al., 1997; Xing et al., 1997; Rojas et al., 2010). These observations are consistent with our present results demonstrating Nurr1 protein expression in a subpopulation of cortical neurons in the intact hemisphere. Precedent studies also reported that Nurr1 expression in specific brain regions was upregulated under several pathological conditions including seizures (Xing et al., 1997), depression-inducing stress (Rojas et al., 2010) and ischemic stroke (Honkaniemi

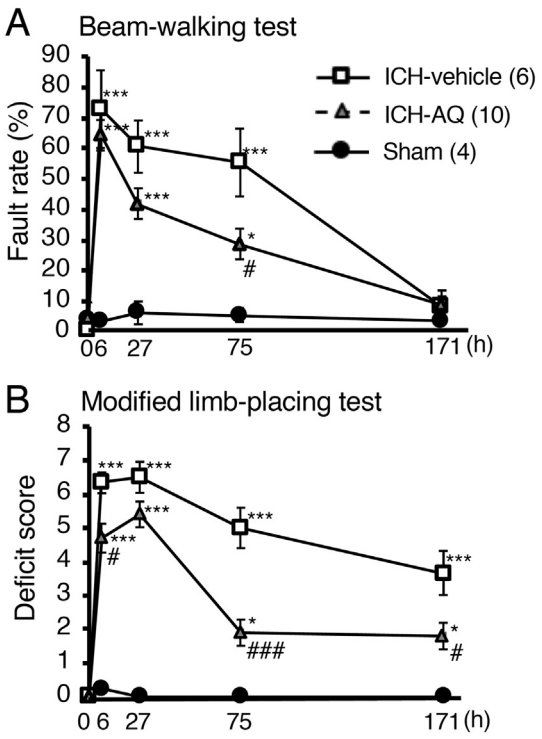

Fig. 6. Amodiaquine improves motor performance after ICH induction.
Amodiaquine (AQ; 40 mg/kg, i.p.) or vehicle was administered 3 h, 27 h and 51 h after induction of ICH, and motor performance of mice was examined at designated time after ICH by the fault rate of hindlimb in the beam-walking test (A) and the deficit score in the modified limb placing test (B).
Number of animals in each group is given in parentheses. * $P < .05$, *** $P < 0.001$ vs. sham group; # $P < 0.05$, ### $P < 0.001$ vs. vehicle group.

et al., 1997). Our present results provide an additional case of Nurr1 upregulation under pathological conditions, but a notable finding was that Nurr1 upregulation after ICH occurred prominently in non-neuronal cells in the perihematomal region, rather than in neurons. This is in contrast with the other cases, for example, seizure-induced Nurr1 upregulation in dentate granule neurons (Xing et al., 1997). However, microglia in primary culture exhibit increased expression of Nurr1 in response to LPS (Fan et al., 2009), and primary astrocytes respond to IL-1β and tumor necrosis factor (TNF) α by Nurr1 upregulation (Saijo et al., 2009). Upregulated expression of Nurr1 in microglia/macrophages and astrocytes might be involved in self-regulation of activation status of these cells. Indeed, Saijo et al. (2009) have shown that Nurr1 knockdown in the midbrain substantia nigra exacerbated LPS-induced expression of inflammatory mediators such as IL-1β and TNFα. Moreover, Nurr1 knockdown in microglial cell line and primary astrocytes also exacerbated expression of inflammatory mediators (Saijo et al., 2009).

Amodiaquine is a traditional anti-malarial drug but has recently been re-identified as a Nurr1 agonist (Kim et al., 2015). Biological actions of this drug in the central nervous system have so far been addressed in a rat model of Parkinson's disease based on 6-hydroxydopamine-induced dopaminergic neurodegeneration (Kim et al., 2015) and in adult hippocampal neurogenesis in mice (Kim et al., 2016). Because amodiaquine was intraperitoneally administered twice daily with at 20 mg/kg in these previous studies, we used a comparable dose of amodiaquine in the present study, that is, daily intraperitoneal injection at 40 mg/kg. Amodiaquine is well known to induce liver injury and agranulocytosis as adverse reactions. In this context, liver injury was induced by oral intake of amodiaquine at 200–300 mg/kg/d with a delayed onset of at least 1 week in female C57BL/6 mice, and the same treatment did not induce liver injury in male mice (Metushi et al., 2015). Concerning agranulocytosis, 14-d treatment with amodiaquine at 5–15 mg/kg did not affect hematological parameters in Sprague-Dawley rats (Saka et al., 2012). Overall, we consider that our dosing regimen (three times daily at 40 mg/kg) produces minimal toxicological problems in mice in the present study. However, toxicological issues on amodiaquine should be considered carefully in the case of translation to human therapy.

With this dosing regimen, we could observe significant suppression by amodiaquine of accumulation of morphologically activated microglia/macrophages and astrocytes in the perihematomal region. Anti-inflammatory effect of amodiaquine was evident also in its suppressive effect on inflammatory cytokine/chemokine expression. Both IL-1β and CCL2 play an important role in the pathogenic events of ICH (Masada et al., 2001; Yao and Tsirka, 2012), and we have previously reported that CXCL2 upregulation is a key factor in ICH pathogenesis (Matsushita et al., 2014). In the present study, induced expression of these inflammatory mediators was found to be suppressed by amodiaquine, suggesting that the anti-inflammatory effects lead to the beneficial consequences of amodiaquine administration such as amelioration of neurological functions. In this context, amodiaquine as well as another Nurr1 ligand C-DIM12 has been shown to suppress gene expression of inflammatory mediators including IL-1β and CCL2 in LPS-stimulated microglial BV-2 cells (De Miranda et al., 2015a; Kim et al., 2015).

Another cytokine whose expression we addressed was IL-15, which has been described as an astrocyte-derived cytokine involved in ischemic brain injury (Li et al., 2017). Amodiaquine only modestly diminished ICH-induced expression of IL-15 mRNA, although astrocyte activation as determined by GFAP immunoreactivity was clearly inhibited by this drug. Because astrocyte activation may play various roles in stroke-associated pathological events (Sims and Yew, 2017), the effect of amodiaquine on astrocyte functions in the perihematomal region may deserve further investigations to reveal its detailed pharmacological profiles.

As in the case with peripheral macrophages, microglia are considered to exhibit different activation/polarization states during the course of sequential pathological processes in the brain, which controls the overall consequences of brain tissue injury (Lan et al., 2017). Particularly in the case with ICH, hematoma resolution by phagocytic activities of microglia/macrophages may help improving the recovery of neurological functions by promoting brain tissue repair (Chang et al., 2017). Indeed, agonists at peroxisome proliferator-activated receptor γ, a member of nuclear receptor family, promote hematoma resolution by microglia/macrophages, thereby improve functional recovery (Chang et al., 2017; Zhao et al., 2007). In the present study, we observed spontaneous hematoma resolution as a time-dependent decrease in the injury volume. We also observed that amodiaquine treatment did not significantly affect the rate of hematoma resolution, suggesting that phagocytic activities of microglia/macrophages were not affected by the drug.

Another line of observations to help understanding the action profiles of amodiaquine was that the drug minimally affected the survival of neurons within the hematoma. Nevertheless, amodiaquine markedly improved the recovery of motor functions of mice after ICH. Overall, our present results suggest that suppressed activation of microglia/macrophages and resultant suppression of production of inflammatory mediators, rather than the alteration in hematoma resolution or neuronal survival, are closely associated with the functional recovery promoted by amodiaquine. However, there remains a possibility that the actions of amodiaquine on Nurr1-expressing neuronal populations, such as regulation of neuronal activity or modulation of neuronal functions, contribute to the mitigation of neurological deficits associated with ICH. In this context, the effect of amodiaquine on an experimental rat model of Parkinson's disease has been reported to involve upregulation of genes specific for dopaminergic neurons as well as downregulation of pro-inflammatory genes (Kim et al., 2015).

At present, we cannot totally exclude the possibility that unidentified molecular targets other than Nurr1 are involved in the beneficial effects of amodiaquine on ICH pathology. However, upregulation of Nurr1 in activated inflammatory cells and the prominent effect of amodiaquine in suppression of inflammatory responses, together with the findings by other groups showing regulatory roles of Nurr1 in brain inflammation, are all consistent with the view that the effect of amodiaquine on ICH is primarily mediated by Nurr1. Further investigations using other kinds of Nurr1 ligands may help confirming the validity of Nurr1 as a novel target for ICH therapy. In addition, the focus of the present study was to address whether amodiaquine could alleviate brain injury and inflammatory responses during the acute phase of the disease, and we examined the effect of amodiaquine up to 7 days after induction of ICH. Therefore, long-term outcome by amodiaquine or other Nurr1 ligands may deserve further investigations by employing longer period of drug administration.

Conflict of interest

The authors declare no conflicts of interest.

Acknowledgments

This work was supported by The Smoking Research Foundation; JSPS KAKENHI, MEXT, Japan [Grants 16H04673, 16K15204]; and Program for Leading Graduate Schools “HIGO (Health life science: Interdisciplinary and Glocal Oriented), MEXT, Japan.

References

Anan, J., Hijioka, M., Kurauchi, Y., Hisatsune, A., Seki, T., Katsuki, H., 2017. Cortical hemorrhage-associated neurological deficits and tissue damage in mice are ameliorated by therapeutic treatment with nicotine. J. Neurosci. Res. 95, 1838–1849.

Bäckman, C., Perlmann, T., Wallén, A., Hoffer, B.J., Morales, M., 1999. A selective group of dopaminergic neurons express Nurr1 in the adult mouse brain. Brain Res. 851, 125–132.

Chang, C.F., Wan, J., Li, Q., Renfroe, S.C., Heller, N.M., Wang, J., 2017. Alternative activation-skewed microglia/macrophages promote hematoma resolution in experimental intracerebral hemorrhage. Neurobiol. Dis. 103, 54–69.

Cordonnier, C., Demchuk, A., Ziai, W., Anderson, C.S., 2018. Intracerebral haemorrhage: current approaches to acute management. Lancet. 392, 1257–1268.

De Miranda, B.R., Popichak, K.A., Hammond, S.L., Jorgensen, B.A., Phillips, A.T., Safe, S., Tjalkens, R.B., 2015a. The Nurr1 activator 1,1-bis(3'-Indolyl)-1-(p-chlorophenyl) methane blocks inflammatory gene expression in BV-2 microglial cells by inhibiting nuclear factor κB. Mol. Pharmacol. 87, 1021–1034.

De Miranda, B.R., Popichak, K.A., Hammond, S.L., Miller, J.A., Safe, S., Tjalkens, R.B., 2015b. Novel para-phenyl substituted diindolylmethanes protect against MPTP neurotoxicity and suppress glial activation in a mouse model of Parkinson's disease. Toxicol. Sci. 143, 360–373.

Fan, X., Luo, G., Ming, M., Pu, P., Li, L., Yang, D., Le, W., 2009. Nurr1 expression and its modulation in microglia. Neuroimmunomodulation. 16, 162–170.

Hijioka, M., Anan, J., Ishibashi, H., Kurauchi, Y., Hisatsune, A., Seki, T., Koga, T., Yokomizo, T., Shimizu, T., Katsuki, H., 2017. Inhibition of leukotriene B_4 action mitigates intracerebral hemorrhage-associated pathological events in mice. J. Pharmacol. Exp. Ther. 360, 399–408.

Honkaniemi, J., States, B.A., Weinstein, P.R., Espinoza, J., Sharp, F.R., 1997. Expression of zinc finger immediate early genes in rat brain after permanent middle cerebral artery occlusion. J. Cereb. Blood Flow Metab. 17, 636–646.

Inamoto, T., Papineni, S., Chintharlapalli, S., Cho, S.D., Safe, S., Kamat, A.M., 2008. 1,1-Bis(3′-indolyl)-1-(p-chlorophenyl)methane activates the orphan nuclear receptor Nurr1 and inhibits bladder cancer growth. Mol. Cancer Ther. 7, 3825–3833.

Kim, C.H., Han, B.S., Moon, J., Kim, D.J., Shin, J., Rajan, S., Nguyen, Q.T., Sohn, M., Kim, W.G., Han, M., Jeong, I., Kim, K.S., Lee, E.H., Tu, Y., Naffin-Olivos, J.L., Park, C.H., Ringe, D., Yoon, H.S., Petsko, G.A., Kim, K.S., 2015. Nuclear receptor Nurr1 agonists enhance its dual functions and improve behavioral deficits in an animal model of Parkinson's disease. Proc. Natl. Acad. Sci. U. S. A. 112, 8756–8761.

Kim, J.I., Jeon, S.G., Kim, K.A., Kim, Y.J., Song, E.J., Choi, J., Ahn, K.J., Kim, C.J., Chung, H.Y., Moon, M., Chung, H., 2016. The pharmacological stimulation of Nurr1 improves cognitive functions via enhancement of adult hippocampal neurogenesis. Stem Cell Res. 17, 534–543.

Lan, X., Han, X., Li, Q., Yang, Q.W., Wang, J., 2017. Modulators of microglial activation and polarization after intracerebral haemorrhage. Nat. Rev. Neurol. 13, 420–433.

Law, S.W., Conneely, O.M., DeMayo, F.J., O'Malley, B.W., 1992. Identification of a new brain-specific transcription factor, NURR1. Mol. Endocrinol. 6, 2129–2135.

Le, W., Conneely, O.M., He, Y., Jankovic, J., Appel, S.H., 1999. Reduced Nurr1 expression increases the vulnerability of mesencephalic dopamine neurons to MPTP-induced injury. J. Neurochem. 73, 2218–2221.

Li, M., Li, Z., Yao, Y., Jin, W.N., Wood, K., Liu, Q., Shi, F.D., Hao, J., 2017. Astrocyte-derived interleukin-15 exacerbates ischemic brain injury via propagation of cellular immunity. Proc. Natl. Acad. Sci. U. S. A. 114, E396–E405.

Masada, T., Hua, Y., Xi, G., Yang, G.Y., Hoff, J.T., Keep, R.F., 2001. Attenuation of intracerebral hemorrhage and thrombin-induced brain edema by overexpression of interleukin-1 receptor antagonist. J. Neurosurg. 95, 680–686.

Matsushita, H., Hijioka, M., Hisatsune, A., Isohama, Y., Shudo, K., Katsuki, H., 2011. A retinoic acid receptor agonist Am80 rescues neurons, attenuates inflammatory reactions, and improves behavioral recovery after intracerebral hemorrhage in mice. J. Cereb. Blood Flow Metab. 31, 222–234.

Matsushita, H., Hijioka, M., Ishibashi, H., Anan, J., Kurauchi, Y., Hisatsune, A., Seki, T., Shudo, K., Katsuki, H., 2014. Suppression of CXCL2 upregulation underlies the therapeutic effect of the retinoid Am80 on intracerebral hemorrhage in mice. J. Neurosci. Res. 92, 1024–1034.

Metushi, I.G., Cai, P., Dervovic, D., Liu, F., Lobach, A., Nakagawa, T., Uetrecht, J., 2015. Development of a novel mouse model of amodiaquine-induced liver injury with a delayed onset. J. Immunotoxicol. 12, 247–260.

Michell-Robinson, M.A., Touil, H., Healy, L.M., Owen, D.R., Durafourt, B.A., Bar-Or, A., Antel, J.P., Moore, C.S., 2015. Roles of microglia in brain development, tissue maintenance and repair. Brain 138, 1138–1159.

Perlmann, T., Wallén-Mackenzie, A., 2004. Nurr1, an orphan nuclear receptor with essential functions in developing dopamine cells. Cell Tissue Res. 318, 45–52.

Rojas, P., Joodmardi, E., Perlmann, T., Ogren, S.O., 2010. Rapid increase of Nurr1 mRNA expression in limbic and cortical brain structures related to coping with depression-like behavior in mice. J. Neurosci. Res. 88, 2284–2293.

Saijo, K., Winner, B., Carson, C.T., Collier, J.G., Boyer, L., Rosenfeld, M.G., Gage, F.H., Glass, C.K., 2009. A Nurr1/CoREST pathway in microglia and astrocytes protects dopaminergic neurons from inflammation-induced death. Cell 137, 47–59.

Saka, W.A., Akhigbe, R.E., Akinola, A.O., Azeez, O.M., 2012. Hematoxicity of amodiaquine in Sprague-Dawley rats. Toxicol. Int. 19, 112–114.

Sims, N.R., Yew, W.P., 2017. Reactive astrogliosis in stroke: contributions of astrocytes to recovery of neurological function. Neurochem. Int. 107, 88–103.

Wang, Z., Benoit, G., Liu, J., Prasad, S., Aarnisalo, P., Liu, X., Xu, H., Walker, N.P., Perlmann, T., 2003. Structure and function of Nurr1 identifies a class of ligand-independent nuclear receptors. Nature 423, 555–560.

Xing, G., Zhang, L., Zhang, L., Heynen, T., Li, X.L., Smith, M.A., Weiss, S.R., Feldman, A.N., Detera-Wadleigh, S., Chuang, D.M., Post, R.M., 1997. Rat nurr1 is prominently expressed in perirhinal cortex, and differentially induced in the hippocampal dentate gyrus by electroconvulsive vs. kindled seizures. Brain Res. Mol. Brain Res. 47, 251–261.

Yao, Y., Tsirka, S.E., 2012. The CCL2-CCR2 system affects the progression and clearance of intracerebral hemorrhage. Glia 60, 908–918.

Zetterström, R.H., Solomin, L., Jansson, L., Hoffer, B.J., Olson, L., Perlmann, T., 1997. Dopamine neuron agenesis in Nurr1-deficient mice. Science 276, 248–250.

Zhao, X., Sun, G., Zhang, J., Strong, R., Song, W., Gonzales, N., Grotta, J.C., Aronowski, J., 2007. Hematoma resolution as a target for intracerebral hemorrhage treatment: role for peroxisome proliferator-activated receptor gamma in microglia/macrophages. Ann. Neurol. 61, 352–362.

Zhou, Y., Wang, Y., Wang, J., Anne Stetler, R., Yang, Q.W., 2014. Inflammation in intracerebral hemorrhage: from mechanisms to clinical translation. Prog. Neurobiol. 115, 25–44.